THE JOURNAL OF BIOLOGICAL CHEMISTRY VOL. 283, NO. 13, pp. 8153–8163, March 28, 2008

The Mechanism of the Reverse Recovery Step, Phosphate Release, and Actin Activation of *Dictyostelium* Myosin II*[S]

Received for publication, October 26, 2007, and in revised form, January 10, 2008 Published, JBC Papers in Press, January 21, 2008, DOI 10.1074/jbc.M708863200

Máté Gyimesi[‡], Bálint Kintses[‡], Andrea Bodor[§], András Perczel[¶], Stefan Fischer[‖], Clive R. Bagshaw[1], and András Málnási-Csizmadia[‡2]**

*From the [‡]Department of Biochemistry, Institute of Biology, the [§]Laboratory of Structural Chemistry and Biology, Institute of Chemistry, and the [¶]Protein Modelling Group MTA-ELTE, Institute of Chemistry, Eötvös University, Pázmány Péter sétány 1/A, Budapest H-1117, Hungary, the [‖]Computational Biochemisry, Interdisciplinary Center for Scientific Computing, University of Heidelberg, Heidelberg 69120, Germany, and the **Department of Biochemistry, University of Leicester, Lancaster Road, Leicester LE1 9HN, United Kingdom*

The rate-limiting step of the myosin basal ATPase (*i.e.* in absence of actin) is assumed to be a post-hydrolysis swinging of the lever arm (reverse recovery step), that limits the subsequent rapid product release steps. However, direct experimental evidence for this assignment is lacking. To investigate the binding and the release of ADP and phosphate independently from the lever arm motion, two single tryptophan-containing motor domains of *Dictyostelium* myosin II were used. The single tryptophans of the W129+ and W501+ constructs are located at the entrance of the nucleotide binding pocket and near the lever arm, respectively. Kinetic experiments show that the rate-limiting step in the basal ATPase cycle is indeed the reverse recovery step, which is a slow equilibrium step ($k_{forward} = 0.05\ s^{-1}$, $k_{reverse} = 0.15\ s^{-1}$) that precedes the phosphate release step. Actin directly activates the reverse recovery step, which becomes practically irreversible in the actin-bound form, triggering the power stroke. Even at low actin concentrations the power stroke occurs in the actin-attached states despite the low actin affinity of myosin in the pre-power stroke conformation.

The mechanism of the phosphate (P_i) release of the myosin ATPase is of particular interest, because it is the key step that is presumed to be activated by actin and is coupled to the working stroke of the cross-bridge cycle (1, 2). The observed rate of phosphate release in the absence of actin is of the order of 0.05 s^{-1} for rabbit skeletal muscle myosin II at 20 °C and provides the major contribution to the rate of the overall basal ATPase activity. Phosphate binding is, however, weak ($K_d > 1$ mM), which led Trentham *et al.* (3, 4) to propose that phosphate release was controlled by a slow isomerization followed by a rapid phosphate release step (*steps 4* and *5* in Scheme 1, respectively). This suggestion was made on the grounds that the second-order rate constant for phosphate binding would be abnormally low if steps 4 and 5 were combined into a single step.

This idea was supported by the experiments of Mannherz *et al.* (5) who demonstrated that a small amount of labeled M*·ATP[3] could be synthesized by the addition of millimolar concentrations of ^{32}P-labeled phosphate to myosin subfragment 1 (S1) in the presence of saturating ADP. From the kinetics and extent of incorporation, they estimated that the M**·ADP·P_i to M*·ADP·P_i isomerization was slow but freely reversible ($K_4 = 15.6$ at pH 8 and 0.9 at pH 6) while phosphate binding to M*·ADP was weak ($K_5 = 7.3$ mM at pH 8 and 55 mM at pH 6). Subsequently, these authors modified their view (6) and considered that the apparent saturation they observed in ^{32}P incorporation was a consequence of the increase in ionic strength with increasing phosphate concentrations. Their important conclusion about the very high affinity of ATP for myosin in the M*·ATP complex was unaffected by this problem, but the values of K_4 and K_5 could no longer be reliably disentangled. Thus, direct evidence for two steps remains elusive.

It was demonstrated in both solution and fiber experiments (3, 7–9) that phosphate release precedes the release of ADP. The ADP-bound myosin state possesses strong actin binding properties, whereas both ADP and phosphate binding to the active site of myosin results in the weakening of the actin-myosin interaction. It was shown in solution experiments that more than half of the free energy obtained from ATP hydrolysis is liberated during phosphate release (8), therefore this step was suggested to be coupled to the power-generating lever arm movement. However, Goldman & Brenner pointed out that solution kinetics might differ from fiber kinetics (10). They and others demonstrated that in single fiber experiments the power stroke precedes the fast phosphate release step and that the starting state of the power stroke in this case is a weak actin binding A·M·ADP·P_i state (11–14).

It is well known that addition of phosphate analogs, such as BeF_x and AlF_4, to skeletal muscle myosin·ADP complexes, generates an enhancement in tryptophan fluorescence, indicative

* This work was supported in part by National Office for Research and Technology (Grants RET 14/2005 and OTKA TS49812 to A. M. C.) and by the Hungarian National Research Foundation (Grant D48459 to B. A.). The costs of publication of this article were defrayed in part by the payment of page charges. This article must therefore be hereby marked "*advertisement*" in accordance with 18 U.S.C. Section 1734 solely to indicate this fact.

[S] The on-line version of this article (available at http://www.jbc.org) contains supplemental text and Figs. S1–S5.

[1] Supported by the Biotechnology and Biological Sciences and Research Council.

[2] To whom correspondence should be addressed. Tel.: 36-1-209-0555/8780; Fax: 36-1-381-2172; E-mail: malna@elte.hu.

[3] The abbreviations used are: M*, enhanced fluorescent state of myosin S1 (~5%); M**, enhanced fluorescent state of myosin S1 (~15%); S1, subfragment 1; dmATP, 3′-(*N*-methylanthraniloyl)-2′-deoxy-ATP; dmADP, 3′-(*N*-methylanthraniloyl)-2′-deoxy-ADP; *Dd*, *D. discoideum*; mant, *N*-methylanthraniloyl.

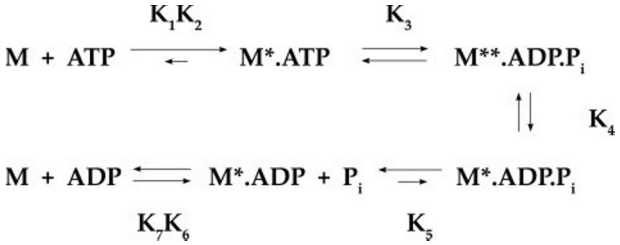

SCHEME 1

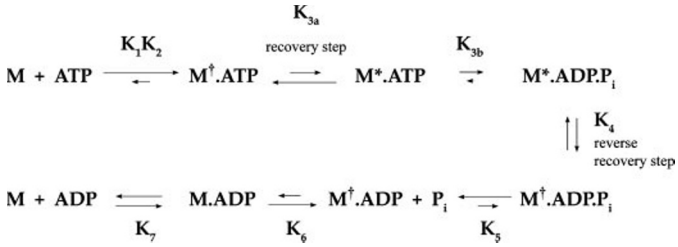

SCHEME 2

of formation of the M** conformation (15). However, attempts to generate the M** state by addition of phosphate at high concentrations to rabbit skeletal muscle myosin S1 in the presence of ADP failed to develop the high fluorescence state. Indeed the protein fluorescence signal decreased and indicated that M·P_i binary complexes formed at the expense of M*·ADP (16). Nevertheless, the results of ^{32}P incorporation show that some M**·ADP·P_i must be generated under these conditions (5, 6). The protein fluorescence of skeletal myosin S1 is sensitive to both nucleotide binding and hydrolysis and probably arises from at least two different tryptophan residues. This contrasts to the situation with the *Dictyostelium discoideum* (*Dd*) myosin II motor domain where there is no enhancement associated with the nucleotide binding steps, because it lacks homologous Trp residues at positions 113 and 131, which are sensitive to the binding events in rabbit myosin (17). Indeed ADP binding gives a small quench in tryptophan fluorescence due to the specific perturbation of Trp-501 (≡Trp-510 in skeletal myosin). We have made a *Dd* motor domain construct, called W501+, which contains only a single tryptophan residue at this conserved position (Fig. 1) and gives an enhanced signal relative to the background compared with the wild-type protein (18–20). In these studies the W501+ construct allowed us to separate the hydrolysis step from the preceding lever arm swing, as is described by Scheme 2.

The labeling in Schemes 1 and 2 are based on different isoforms, skeletal muscle myosin II S1 and W501+ *Dd* myosin motor domain construct, respectively. In Scheme 1, M* represents the partially enhanced fluorescent state of rabbit S1 (reviewed in Ref. 21). This state is equivalent with the $M^{\dagger}$ in Scheme 2, which is a quenched Trp-501 fluorescence state of *Dd* myosin. In the text below we use the nomenclature of Scheme 2, where M* and $M^{\dagger}$ represent the high and the low fluorescence intensity states of Trp-501, respectively (18). The M state corresponds to the apo structure (22, 23). $M^{\dagger}$ corresponds to the pre-recovery state (down lever arm position, see Table 1), in which switch 1 is closed, while switch 2 is open so that the catalytic function of the ATPase is turned off in this state. M* in Scheme 2 (equivalent to M** in Scheme 1) represents the post-recovery state (up lever arm position, see Table 1). During step 3a, the lever arm swing (recovery step) is coupled to the closing of switch 2 (18, 19), thereby activating the ATPase function (24, 25). After ATP hydrolysis (step 3b), step 4 involves the swinging of the lever arm, which we call here the "reverse recovery step." It is important to distinguish the reverse recovery step from the power stroke, because the reverse recovery step is a reversible step in the absence of actin while power stroke occurs in the actin-attached form and exerts force (large free energy change).

All these steps are summarized in Table 1 to clarify the nomenclature we use in this report. We recommend using the recovery step and reverse recovery step instead of using recovery stroke and reverse recovery stroke, because these steps are freely reversible equilibrium steps and occur in the absence of actin. For an effective stroke one object must be in interaction with another object on which it can exert force. From this aspect, in the absence of actin the meaning of stroke is limited, therefore we recommend using the recovery/reverse recovery step for the particular conformational changes.

The mechanism of the reverse recovery step can be either a slow lever arm motion followed by relatively fast product release, or alternatively, the lever arm reorientation is a fast equilibrium step followed by the relatively slow phosphate release step (26). Answering which of these two mechanisms is correct is fundamental regarding the myosin ATPase mechanism, because it defines which is the rate-limiting step that is activated by actin binding during the power stroke: The first case would correspond to an "induced strain" mechanism, in which actin binding provokes a strain in the myosin head, and lever arm motion can release that strain. The second case would correspond to a "Brownian ratchet" mechanism, in which the pre-power stroke lever arm is freely reorienting and product release stabilizes the post-power stroke orientation.

Here we address these questions by characterizing the kinetics of ADP and phosphate binding reactions and the related lever arm swing. The kinetics of these steps are studied as a function of [P_i] at constant ionic strength. We also make comparable studies on a W129+ construct (17) that has a single tryptophan near the active site (Fig. 1), which responds only to nucleotide and phosphate binding but not to the lever arm motion. We present direct experimental evidence first, that ADP and phosphate binding events (*steps 5* and *6* in Scheme 2) are kinetically separate from the reverse recovery step (*step 4*). The reverse recovery step occurs at slow equilibrium, which controls product release and is the rate-limiting step of the basal ATPase cycle (*i.e.* in the absence of actin). However, in the presence of actin the lever arm swing is accelerated by actin binding, thus increasing the ATPase turnover rate. The low initial affinity of M*·ADP·P_i for actin increased during the lever arm swing and the subsequent product release steps, thus depleting the weakly bound A·M*·ADP·P_i population and pulling the reaction toward the actin-bound power stroke.

EXPERIMENTAL PROCEDURES

Unless otherwise stated, all chemical reagents were purchased from Sigma-Aldrich. Nucleotides and dmATP were

TABLE 1

Nomenclature of the enzymatic steps

It is essential to distinguish the post-recovery step conformational state (M*·ATP and M*·ADP·P_i states) from the pre-power-stroke state (A·M*·ADP·P_i). The latter is in the actin-bound conformational state, which is different from the post-recovery step state from both energetic and structural aspects.

Enzymatic steps		Rate constant		Initial and end states of the forward steps (lever arm position/nucleotide form)	
K_1	ATP binding collision step	k_1	Forward	Apo	ATP-binding
		k_{-1}	Reverse	Collision complex with ATP	
K_2	ATP binding-induced conformational change	k_2	Forward	Collision complex with ATP	
		k_{-2}	Reverse	Down[a] ATP state	
K_{3a}	Recovery step[b]	k_{3a}	Forward	Down ATP state	Effective hydrolysis step
		k_{-3a}	Reverse	Up[c] ATP state	
K_{3b}	Hydrolysis step	k_{3b}	Forward	Up ATP state	
		k_{-3b}	Reverse	Up ADP·P_i state	
K_4	Reverse recovery step[d,e]	k_4	Forward	Up ADP·P_i state	
		k_{-4}	Reverse	Down ADP·P_i state	
K_4'	Power stroke	k_4'	Forward	Actin-bound up ADP·P_i state	
		k_{-4}'	Reverse	Actin-bound down state[e]	

[a] The down lever arm state is also called the post-rigor and post-power stroke states, although it also exists in the actin-detached state.
[b] We recommend the nomenclature of the recovery/reverse recovery step instead of the recovery/reverse recovery stroke, because a stroke cannot be explained by an equilibrium step.
[c] The up lever arm state is generally called pre-power stroke state, although it also exists in actin-detached state.
[d] Reverse recovery step is also called the power stroke, even in the absence of actin. We suggest the distinction between the actin-induced power stroke from the reverse recovery step, which occurs in the absence of actin or in the actin-detached form of myosin.
[e] Because the sub-steps of the power stroke have not been resolved in detail, the final state is undefined, as yet.

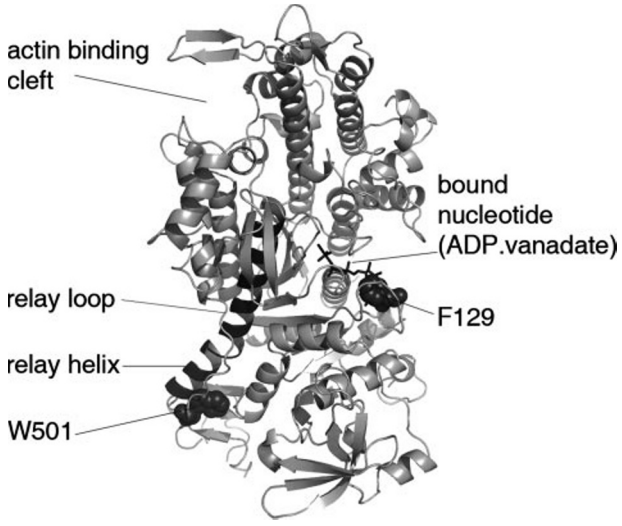

FIGURE 1. **X-ray crystal structure of *Dd* myosin II MD complexed with ADP·vanadate (1VOM).** Trp-501 and Phe-129 residues are rendered in space-filling appearance. W501+ and W129+ motor domain constructs contain single tryptophans at the positions of 501 and 129, respectively. Phe-129 is in close proximity to bound nucleotide (here Mg·ADP·VO_4 is shown as a *black stick*), whereas Trp-501 is located in the relay region.

obtained from Roche Applied Science and Jena Bioscience GmbH, respectively.

Phosphate Buffers—Care was taken to maintain the constant ionic strength in the experiments using different phosphate concentrations or pH. Ionic strength values were calculated according to (27) using the Buffers for pH Control website, and ionic strength was kept constant with additional NaCl to the phosphate buffers.

Reduction of Pyrophosphate Contamination—To reduce the pyrophosphate contamination in the phosphate buffers, 0.5 M Na_2HPO_4 buffer (pH $\leq$ 12.6) was autoclaved at 121 °C for 30 min immediately before the experiments.

Expression and Purification of Proteins—In this study we used *Dd* myosin II motor domain mutants, which are based on the M761 construct (28). The W501+ construct possesses W36F, W432F, and W584F mutations (18), the W129+ construct contains W36F, W432F, W501F, W584F, and F129W mutations (17), and both were cloned into the pDXA-3H vector (29). Both W501+ and W129+ were expressed in *Dd* cells cultured in HL-5 (Formedium) medium at 21 °C and purified as in a previous study (18). After purification proteins were dialyzed against an assay buffer (20 mM HEPES, pH 7.2, 40 mM NaCl, 1 mM $MgCl_2$, 3 mM β-mercaptoethanol, 5 mM benzamidine), and after dialysis, proteins were frozen to liquid nitrogen in 50-μl droplets. Actin was purified as described (30). Protein concentrations were determined with the Bradford method.

Steady-state Kinetic Measurements—Steady-state spectra and time courses of the purified proteins were measured on a FluoroMax SPEX-320 spectrofluorometer. All measurements were carried out at 20 °C. Trp fluorescence was excited at 296 nm with 2 nm bandwidth for both excitation and emission sides, and emission was detected from 305 to 420 nm. Time courses were followed by tryptophan fluorescence exited at 296 nm and detected at 340 nm.

Transient Kinetic Measurements—Stopped-flow measurements were carried out with a KinTek-2004 equipped with a Super Quiet Mercury-Xenon Lamp (Hamamatsu) or with a BioLogic SFM-300/400 stopped-flow fluorometer equipped with a mercury-xenon lamp (Hamamatsu). Trp fluorescence was excited at 297 nm where the mercury-xenon lamp has a discrete emission peak. Slits were adjusted to 2 nm in the case of the KinTek-2004 stopped-flow and a 340 nm interference filter (Corion CFS-001999 9L134) was used on the emission side in both instruments. *N*-Methylanthraniloyl (mant) derivatives were excited either directly at 365 nm or via energy transfer (Forster resonance energy transfer) at 280 nm. In both cases, a WG420 cut-off filter (Comar Instruments) was used to selectively measure mant fluorescence. The cuvette block and the syringe house were thermostatted at 20 °C both in the KinTek 2004 and the BioLogic SFM-300/400 stopped-flow solutions. The dead-time parameter of the KinTek 2004 apparatus at 18 ml/s flow-rate was determined to be 1 ms (31). The BioLogic SFM-300/400 was equipped with an 8-μl cuvette (μFC-08) or a

15-μl cuvette (FC-15), which had <0.2 ms or 2 ms dead time at 18 ml/s, respectively, which increases if slower flow-rate is applied. Unless otherwise noted post-mix concentrations of the reactants are presented.

Actin-activated ATPase Measurement—Actin-activated ATPase activity of W501+ was measured using a pyruvate kinase/lactate dehydrogenase-coupled assay at 20 °C as follows: 2% pyruvate kinase/lactate dehydrogenase enzyme mixture, 1 mM ATP, 1 mM phosphoenolpyruvate, and 200 μM NADH was used in the 5 mM HEPES, 1 mM $MgCl_2$, and 1 mM KCl buffer at pH 7.2, with 0.5 μM W501+ and an actin concentration of 0 to 94 μM.

NMR Spectroscopy—^{31}P NMR spectra were collected at 101.25 MHz on a Bruker Avance 250 spectrometer using a 5-mm inverse $^{1}H/^{13}C/^{31}P/^{19}F$ probe head at room temperature. The inverse-gated proton-decoupling sequence was applied with 4-μs time, 30° pulse, 1-s FID acquisition time, and 1.2-s acquisition delay, and 21,000 scans collected. Chemical shifts were referenced to an external 85% H_3PO_4 standard at 0.00 ppm. All NMR samples were prepared by mixing 0.6 μl of 0.5 M Na_2HPO_4 solution (pH 7.5) and 0.06 μl of D_2O.

RESULTS

Detection and Elimination of Pyrophosphate Traces from Phosphate Buffer—We determined that untreated phosphate buffers contained ~0.01% pyrophosphate contamination (Fig. 2). Because pyrophosphate has high affinity for myosin (K_d,PP_i = 200 nM), even this small concentration of pyrophosphate can block the binding of the substrates with lower affinity such as ADP (K_d,ADP ~ 1 μM) or phosphate (K_d,P_i ~ 10 mM). However, according to the NMR spectroscopy results, heat treatment at alkaline pH (see "Experimental Procedures") can reduce the pyrophosphate level by 5- to 10-fold and enabled us to investigate reactions of myosin and substrates at high phosphate concentrations. A detailed description of the experiments with the related figures (supplemental Fig. S1, *a–c*) can be found in the supplemental materials.

Phosphate Binding of W501+·ADP Complex—To study ligand binding and the possible reverse reaction of the recovery step (M^{+}·ADP·P_i ↔ M*·ADP·P_i), W501+ was preincubated with ADP and then rapidly mixed with different concentrations of a phosphate solution in the stopped-flow apparatus. The ionic strength of the solutions was kept constant in all experiments by adding an appropriate amount of NaCl. Also the ionic strength of the solutions was identical in both syringes of the stopped-flow apparatus. The reactions were studied at I = 244 mM at pH 7.2 and I = 118 mM at pH 7.2 and 6.7. At all phosphate concentrations studied, large and slow fluorescence increases (35% enhancement with k_{obs} = 0.14 s^{-1} at 25 mM phosphate concentration, pH 7.2, I = 118 mM) were detected, which indicates the formation of M*·ADP·P_i. Because the rate constant of ADP release is 5 s^{-1} and accompanied with a 10–15% fluorescence increase, the larger than 15% amplitude increase and the slower than 5 s^{-1} observed rate constants rule out this fluorescence enhancement being simply due to dequenching on displacement of ADP from M^{+}·ADP. Upon phosphate binding to W501+, in the absence of ADP, a small (<3%) quench was detected. At each applied ionic strength and pH, stopped-flow

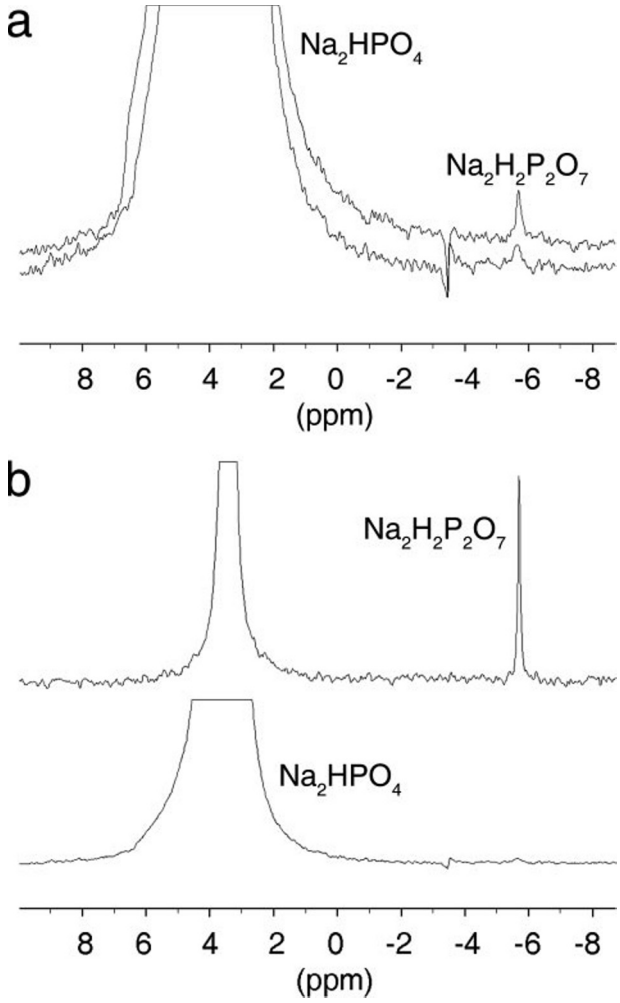

FIGURE 2. **Determination of the contaminating pyrophosphate traces in phosphate buffer by NMR spectroscopy.** *a*, $^{31}P\{^{1}H\}$ NMR spectra of samples containing 0.6 μl of 0.5 M NaH_2PO_4 (pH 7.5) and 0.06 μl of D_2O. The *bottom spectrum* belongs to the boiled and the *top spectrum* to the non-treated solution demonstrating that boiling the buffer for 30 min at 121 °C in an autoclave can reduce the pyrophosphate level 5- to 10-fold. *b*, $^{31}P\{^{1}H\}$ NMR spectra of samples containing 0.6 μl of boiled 0.5 M NaH_2PO_4 solution (pH 7.5) and 0.06 μl of D_2O, recorded with 21,000 scans (*bottom*), and after addition to this solution of 30 μl of 0.1 M $Na_2H_4P_2O_7$ (pH 7.5), recorded with 54 scans (*top*). This experiment demonstrates that the contaminating compound in phosphate buffer, which can be reduced by heat treatment, is pyrophosphate.

records could be fitted with single exponentials (Fig. 3*a*). In addition, a very slow (0.005 s^{-1}) fluorescence quench also was observed that is the consequence of binding of residual pyrophosphate. This reaction was faster and became dominant when untreated phosphate samples were used (see supplemental Fig. S1*c*). The amplitudes and the observed rate constants of the fluorescence enhancement increased with phosphate concentrations. The slope of the initial linear fit of the plot of rate constants *versus* phosphate concentration ($k^{W501+\cdot ADP}_{Pi,on,app,118mM,pH7.2}$ = 0.0036 $mM^{-1}s^{-1}$) depends on both the ionic strength and pH (Fig. 3*b*), whereas the extrapolated intercepts ($k^{W501+\cdot ADP}_{Pi,on,app,118mM,pH7.2}$ = 0.052 s^{-1}) were practically unchanged. From these values the dissociation constant of phosphate for W501+·ADP complex is K_d,app,P_i = 14.2 mM at 118 mM ionic strength. The intercept value is the same as the basal ATPase rate constant. This indicates that k_{+4} determines the ATPase

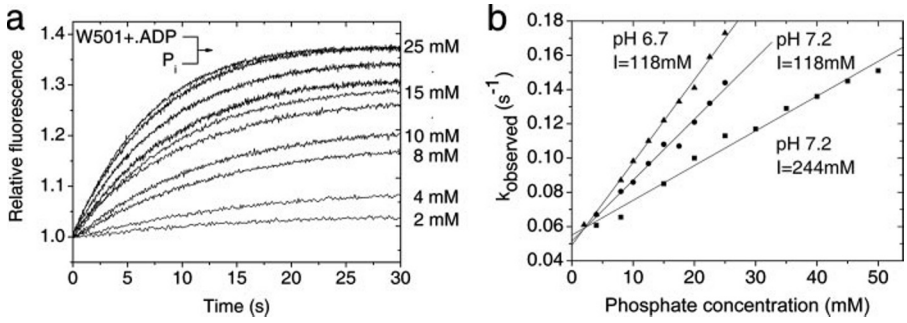

FIGURE 3. **Phosphate binding of W501+·ADP.** *a*, stopped-flow records of 3 μM W501+·ADP complex rapidly mixed with different amount of phosphate (2–25 mM), while the ionic strength (I = 118 mM) and pH (pH 7.2) were kept constant. The large enhancement in fluorescence shows that the M*·ADP·P_i complex develops upon phosphate binding. *b*, plot of the observed rate constants of the reaction (described in *a*) against phosphate concentration at different ionic strengths (I = 118 mM or 244 mM) or pH (pH 6.7 or 7.2). From this plot the on- and off-rate constants of phosphate binding sensed by Trp-501 can be calculated: $k^{W501+\cdot ADP}_{Pi,on,app,118\ mM,pH7.2}$ = 0.0036 $mM^{-1}s^{-1}$ and $k^{W501+\cdot ADP}_{Pi,off,app,118\ mM,pH7.2}$ = 0.052 s^{-1} (other parameters are shown in Table 2).

TABLE 2

Summary of the rate and equilibrium constants measured in this study

Each section shows the experiment from which the values are originated. (Arrangement of stopped-flow reactions are simplified as: component(s) in one syringe × component in the other syringe.)

	Measured constants
W501+·ADP × P_i	
P_i half sat (I = 118 mM, pH 6.7)	12 mM
P_i half sat (I = 118 mM, pH 7.2)	14.2 mM
P_i half sat (I = 244 mM, pH 7.2)	23 mM
$k_{on,Pi}$ (I = 118 mM, pH 6.7)	0.0048 $mM^{-1}s^{-1}$
$k_{on,Pi}$ (I = 118 mM, pH 7.2)	0.0036 $mM^{-1}s^{-1}$
$k_{on,Pi}$ (I = 244 mM, pH 7.2)	0.0020 $mM^{-1}s^{-1}$
$k_{off,Pi}$ (I = 118 mM, pH 6.7)	0.049 s^{-1}
$k_{off,Pi}$ (I = 118 mM, pH 7.2)	0.052 s^{-1}
$k_{off,Pi}$ (I = 244 mM, pH 7.2)	0.055 s^{-1}
$k_{max,Pi}$ (I = 118 mM, pH 7.2)	~0.2 s^{-1}
$K_d$app,P_i (I = 118 mM, pH 7.2)	14.2 mM
W501+·P_i × ADP	
$K_d$app,ADP	45 μM
$K_{on,ADP}$	0.011 $\mu M^{-1}s^{-1}$
$k_{max,ADP}$	0.2 s^{-1}
W129+·P_i × ADP	
ADP,half sat	15 μM
$k_{PD,on}$	1.6 $\mu M^{-1}s^{-1}$
$k_{PD,off}$	19 s^{-1}
$k_{max,ADP}$	370 s^{-1}
W129+·ADP × P_i	
k_{obs}	7.5 ± 1 s^{-1}
W129+ × P_i	
$k_{fast,on,Pi}$ [a]	50.3 $mM^{-1}s^{-1}$
$k_{fast,off,Pi}$ [a]	35.0 s^{-1}
$k_{fast,max,Pi}$ [a]	300 s^{-1}
k_{slow} [a]	5 s^{-1}
W129+ × ATP	
$k_{ATP,fast}$	1140 s^{-1}
$k_{ATP,slow}$	350 s^{-1}
W129+·P_i × ATP	
$k_{P,off}$	260 s^{-1}
W501+·dmADP × ATP	
k_{obs}	2.5 s^{-1}
W501+·dmADP·P_i × ATP	
k_{fast}	5.8 s^{-1}
k_{slow}	0.04 s^{-1}
A_{fast}/A_{slow}	0.50
W501+ × ADP	
$k_{D,on}$	1.2 μM^{-1}
$k_{D,off}$	7 s^{-1}
K_D (K_{dD})	0.17 μM^{-1} (5.8 μM)
W501+·ADP·AlF4 × PyA	
K_d, A·M*·ADP·P_i	57 μM

[a] Results can be found in the supplemental material.

rate constant of the cycle. It also supports the conclusion that the M*·ADP·P_i state is the one generated by addition of ADP and phosphate to W501+. The parameters under other conditions are presented in Table 2. Because the increase of phosphate concentration was limited by the constant ionic strength of the solution, it could not be increased above 25 mM at pH 7.2, therefore the saturation of values of rate constants could not be determined. Furthermore, it is difficult to characterize these values, because rate constants are strongly dependent on ionic strength and it is hard to maintain a constant value with different counter ions. Even a little overcompensation of the ionic strength level with sodium chloride could cause the apparent saturation of the observed rate constant. In summary, there is some indications that the rate constant might saturate at around $k^{W501+\cdot ADP}_{Pi,max,app} \approx 0.2\ s^{-1}$. To overcome this uncertainty we carried out the inverse experiment in which W501+ was premixed with phosphate and then rapidly mixed with ADP.

ADP Binding of W501+·P_i Complex—W501+ was preincubated with 25 mM phosphate at pH 7.2 and rapidly mixed in the stopped-flow apparatus with different concentration of ADP. Both stopped-flow syringes contained 25 mM phosphate to keep phosphate concentration constant at pH 7.2 and I = 118 mM. Figs. 4*a* and 6 show a stopped-flow record of the reaction of W501+·P_i complex with 350 μM ADP. A small (5%) and fast (400 s^{-1}) fluorescence quench was followed by a 25% fluorescence increase. The apparent rate constant of the fluorescence increase depended on the ADP concentration (Fig. 4*b*), the initial slope of the plot is $k^{W501+\cdot Pi}_{ADP,on,app}$ = 0.011 $\mu M^{-1}s^{-1}$. The observed rate constant of the reaction saturated at $k^{W501+\cdot Pi}_{ADP,max,app}$ = 0.20 s^{-1}, which is a similar value to the estimated maximum rate constant of phosphate binding of W501+·ADP complex ($k^{W501+\cdot ADP}_{Pi,max,app} \approx 0.2\ s^{-1}$).

ADP Binding of W129+·P_i Complex—In contrast to Trp-501, which senses the lever arm swing, Trp-129 is sensitive to the binding events of ligands (17, 18). The fluorescence of Trp-129 is quenched by all adenosine nucleotides (ADP, ATP, and ADP·P_i) and its phosphate analog (ADP·AlF_4) by 55%, whereas phosphate binding slightly (10%) increases its fluorescence. Using W501+ and W129+, we can potentially distinguish the lever arm swing from product binding events if the kinetics is favorable. When 4 μM W129+ was mixed with different concentrations of ADP (pH 7.2, I = 118 mM) in the presence of a saturating amount of phosphate, a large fluorescence quench was detected (Figs. 5 and 6). Single exponentials were fitted to all records. Increasing the ADP concentration increased both the amplitudes and the observed rate constants of the fluorescence changes. At higher ADP concentrations the rate constant was so high that significant amplitude loss occurred during the dead time of the stopped-flow apparatus. A hyperbola was fitted to the plot of rate constants *versus* ADP concentration, which yielded an initial slope, $k^{W129+\cdot Pi}_{ADP,on,app}$ = 1.6 $\mu M^{-1}s^{-1}$ and an intercept (extrapolated observed rate constant at zero ADP concentration), $k^{W129+\cdot Pi}_{ADP,off,app}$ = 19 s^{-1}. The hyperbola saturates

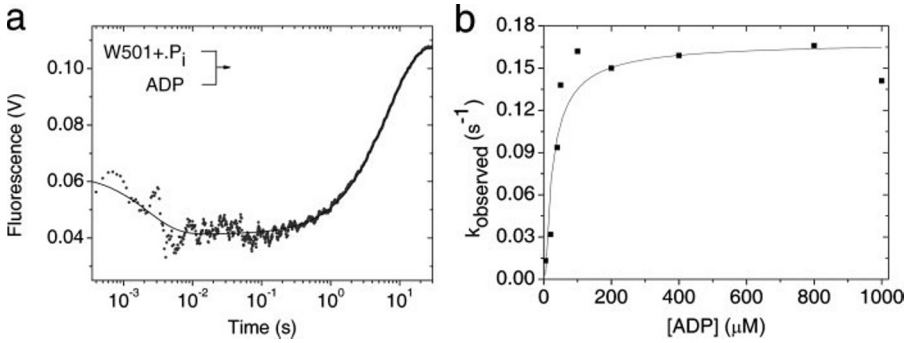

FIGURE 4. **ADP binding of W501+ in the presence of phosphate.** *a*, stopped-flow record of 3 μM W501+ mixed with 350 μM ADP in the presence of 25 mM phosphate on both sides. A fast (400 s^{-1}) quenching phase with small amplitude change (5%) is followed by an [ADP]-dependent slow (0.2 s^{-1}) increasing phase. This experiment also confirms that, in the presence of ADP and phosphate, the closed (Trp-501 high fluorescence) state can be developed. *b*, plot of the observed rate constants of the ADP binding to W501+·P_i complex. The fitted hyperbola saturated at $k^{W501+\cdot Pi}_{ADP,max,app} = 0.20\ s^{-1}$.

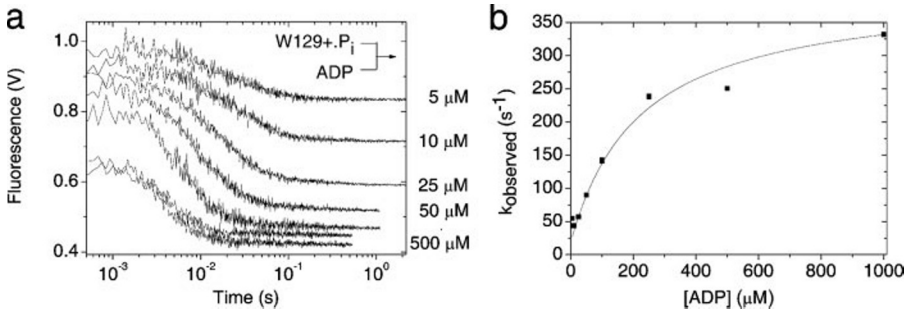

FIGURE 5. **ADP binding of W129+ in the presence of phosphate.** *a*, stopped-flow records of the ADP binding reaction of 4 μM W129+ in the presence of 25 mM phosphate. The fluorescence quench sensed by Trp-129 responds to the nucleotide binding. Note that ADP binding to M·P_i complex results in a fast fluorescent decrease in the case of W129+ but causes a slow fluorescence enhancement in the W501+. At high ADP concentrations significant amplitude is lost in the dead time of the stopped-flow. *b*, single exponentials were fitted to the traces and the observed rate constants were plotted against [ADP], which showed the maximal rate constant for the reaction is $k^{W129+\cdot Pi}_{ADP,max,app} = 370\ s^{-1}$. The on- and off-rate constants of ADP binding to M·P_i was calculated from the initial slope and the intercept of the fitted hyperbola, respectively: $k^{W129+\cdot Pi}_{ADP,on,app} = 1.6\ \mu M^{-1}s^{-1}$ and $k^{W129+\cdot Pi}_{ADP,off,app} = 19\ s^{-1}$.

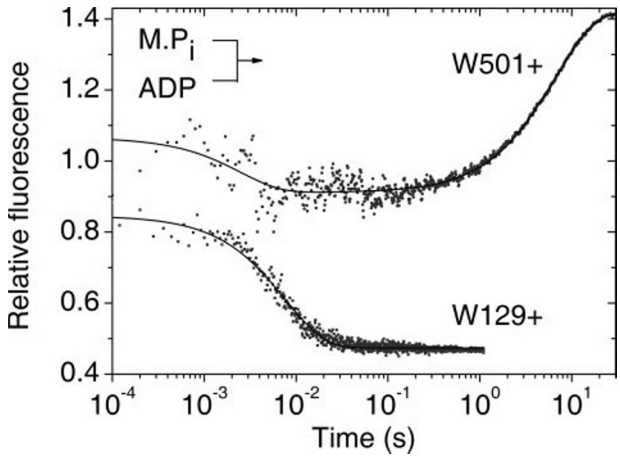

FIGURE 6. **Stopped-flow records of ADP binding to the M·P_i complex for W501+ (*upper trace*) and W129+ (*lower trace*).** Please note that the data used here are from Figs. 3 and 4. They are normalized to a starting fluorescence of 1 to make the amplitudes comparable. Trp-129 responds to ADP binding to W129+·P_i with a fast fluorescence quench (~150 s^{-1} at 100 μM ADP), whereas the same reaction produces a small fast quench followed by a dominant slow (~0.15 s^{-1} at 350 μM ADP) fluorescence enhancement of Trp-501. This implicates that W129+ is sensitive for the nucleotide binding itself, whereas W501+ senses the large isomerization step coupled with the power stroke of myosin. Using these two mutants allowed us to study the properties of the nucleotide binding pocket separately from the isomerization step.

at the rate constant $k^{W129+\cdot Pi}_{ADP,max,app} = 370\ s^{-1}$, however, it is probably underestimated because of the amplitude loss in the dead time. The half-maximum of the amplitude of the fluorescence change was at $[ADP]^{W129+\cdot Pi}_{half\text{-}sat} = 15\ \mu M$.

Phosphate Binding of W129+·ADP Complex—When W129+·ADP complex was rapidly mixed with phosphate in a stopped-flow apparatus, a small fluorescence change was detected. Because the fluorescence level of W129+·ADP and W129+·ADP·P_i are identical, the small signal change was the consequence of the re-equilibration of the high (apo and W129+·P_i) and the low (W129+·ADP and W129+·ADP·P_i) fluorescence states when the enzyme was not completely saturated with ligands. Supplemental Fig. S2 shows the stopped-flow records of the reaction when 4 μM W129+ was mixed with 50 mM phosphate at pH 7.2, I = 118 mM, while the same ADP concentration was maintained in both syringes. The records show the reactions at four different ADP concentrations (50 μM, 150 μM, 450 μM, and 1 mM). At 1 mM ADP concentration, a 3.5% fluorescence increase was detected whose amplitude increased to 17% at 50 μM ADP concentrations. Single exponentials were fitted to the records. In the range of ADP concentrations studied, the observed rate constants were similar (7.5 $s^{-1} \pm 1\ s^{-1}$) (for more details see supplemental Fig. S2, *a–d*).

Phosphate Binding of W129+—In contrast to W501+, W129+ responds with a small (10–15%) fluorescence increase upon phosphate binding. The kinetics of the signal change when 5 μM W129+ was mixed with different concentration of phosphate were characterized at pH 7.2, I = 118 mM. The records were fitted with double exponentials (supplemental Fig. S3*a*), in contrast to the records of W129+·ADP mixed with phosphate (see above). The observed rate constant of the slow phase was 5 s^{-1} and independent of the phosphate concentrations studied (supplemental Fig. S3*c*). The rate of the fast phase was dependent on and plotted against phosphate concentration and the plot between 0.5 and 5 mM phosphate concentrations was fitted with linear (supplemental Fig. S3*b*). The slope was $k^{W129+}_{Pi,on,app} = 50.3\ mM^{-1}s^{-1}$ and its intercept $k^{W129+}_{Pi,off,app} = 35.0\ s^{-1}$, and the rate constant of the fast phase was maximum at $k^{W129+}_{Pi,max,app} = 300\ s^{-1}$ at 5 mM phosphate concentration and did not exceed 300 s^{-1} even at 25 mM phosphate concentration. We were interested whether this phosphate binding site was part of the functional ATP binding site or an alternative

phosphate binding region sensed by W129+. To test these possibilities, phosphate bound to W129+ was chased by large excess of ATP, and the record was compared with the reaction record when W129+ was mixed with ATP in the absence of phosphate. In the latter reaction the fluorescence change has two phases, as described in an earlier study (17). The observed rate constants of the slow and fast phases were $k^{W129+}_{ATP,slow} = 350\ s^{-1}$ and $k^{W129+}_{ATP,fast} \geq 1000\ s^{-1}$. When motor domain was complexed with phosphate and chased with ATP, the fluorescence change became a single phase and its observed rate constant slowed to $k^{W129+}_{Pi,off,ATPchase} = 260\ s^{-1}$ (supplemental Fig. S4). When W129+ was not saturated with phosphate, a slow and a fast phase could be distinguished. The ratios of the amplitudes of these phases were difficult to determine because of the significant loss of the fast phase in the dead time of the stopped-flow apparatus.

Because the ATP chasing experiment showed a much higher off-rate constant for phosphate than the off-rate constant determined by the intercept in the phosphate binding experiment (260 s^{-1} and 35 s^{-1}, respectively), and also the binding constants differed significantly in these experiments, we suggest that, in the direct P_i binding experiment, an alternative phosphate binding site is involved. This is presumed to be close to the substrate binding pocket, because Trp-129 senses its binding, but it does not overlap with the functional ATP binding site, because ATP does not displace it (*i.e.* there was no slow phase of ATP binding limited by the off-rate constant of 35 s^{-1}).

Dissociation of ADP from M·ADP·P_i by Chasing dmADP—To study the mechanism of the dissociation of ADP and phosphate directly, 8 μM W501+ motor domain was preincubated with 100 μM dmADP (premix concentrations) in the presence and absence of 42 mM phosphate, and the ligands were chased with 2 mM ATP (dmADP was prepared by incubation of dmATP with W501+ for 15 min at 20 °C). In both experiments, the mant fluorescence signal decrease was followed, which is limited by the dissociation of bound dmADP. In the absence of phosphate, a single exponential fitted to the fluorescence record to yield a rate constant, $k_{off,mantADP} = 2.5\ s^{-1}$. The off-rate constant of mantADP is slightly smaller than that of ADP (7 s^{-1}) (17). This effect is caused by the mant group, which interacts with the protein (32), and results in higher affinity of dmADP to myosin (33–35). By contrast, in the presence of phosphate, two phases of displacement were detected. The rate constants of the fast and the slow phases were $k = 5.8\ s^{-1}$ and $k = 0.04\ s^{-1}$, whereas the ratio of their amplitudes was $A_{fast}/A_{slow} = 0.50$ (Fig. 7). The slower rate constant indicates that some M*·dmADP·P_i formed during the preincubation reaction.

Actin Binding of W501+·ADP·AlF_4 Complex—We investigated actin binding of the W501+·ADP·AlF_4 complex by following the light scattering signal. 109 μM W501+ was mixed with 1 mM ADP, 1 mM $AlCl_3$, and 5 mM NaF on ice for 3 h, and the formation of the complex was followed by the fluorescent steady-state emission intensity enhancement of Trp-501. To investigate the actin binding properties of the complex, a varying amount of W501+·ADP·AlF_4 and 1 μM F-actin was mixed in a stopped-flow apparatus and light scattering signal was followed. Very fast reactions (>1000 s^{-1}) were detected even at low W501+·ADP·AlF_4 concentrations, and most of the signal change was lost in the dead time of the stopped-flow apparatus. The signal in the stopped-flow apparatus was so stable that almost all of the single traces overlapped with each other. This enabled us to determine the starting and the endpoints of the reactions at specific W501+·ADP·AlF_4 concentrations where the signal difference represented the total amplitude of the reaction. The amplitudes of the reactions were plotted against W501+ concentration, and the fitted hyperbola resulted in the dissociation constant K_d·AlF_4·actin = 57 μM (supplemental Fig. S5).

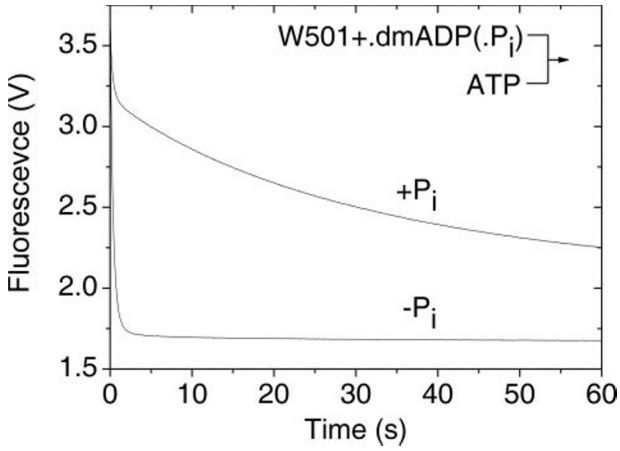

FIGURE 7. **Stopped-flow records of 8 μM W501+ complexed with 100 μM dmADP and mixed with 2 mM ATP in the absence (*lower trace*) or in the presence (*upper trace*) of 42 mM phosphate (premix concentrations).** The fast (2.5 s^{-1}) ADP release step sensed by mant fluorescence enhancement shows single exponential decay in the absence of phosphate, however, in the presence of phosphate the fast phase (5.8 s^{-1}) is followed by a slow (0.04 s^{-1}) phase. The ratio of the amplitudes in the latter case is $A_{fast}/A_{slow} = 0.50$.

Actin-activated ATPase Experiments with W501+—Actin-activated steady-state ATPase activity was measured on W501+ by a pyruvate kinase/lactate dehydrogenase-coupled assay measurement. Activities were determined in the presence of different amount of F-actin and were plotted against actin concentration. The maximum of actin-activated ATPase activity was $v_{max} = 3.8\ s^{-1}$, and half-saturation was determined at $K_m = 67\ \mu M$.

DISCUSSION

In the Bagshaw-Trentham scheme, the relationship between the reverse recovery step (K_4) and the product release steps (K_5, K_6, and K_7) had not been fully resolved. Because Trp-129 and Trp-501 are very sensitive signals for ligand binding and lever arm motion, respectively, the kinetics of the two processes can be investigated separately. To exploit these probes to measure phosphate binding, we found it necessary to minimize pyrophosphate contamination by boiling the stock phosphate solution. It is a well known requirement that vanadate solutions need to be boiled to remove polymeric species before using orthovanadate as phosphate analog for myosin product complex formation (36, 37). However, it is less appreciated that phosphate stock solutions need similar treatment.

With this experimental approach, the mechanism of the basal ATPase activity can be elucidated, and we can compare the processes to the "actin-induced" ATPase mechanism. In the

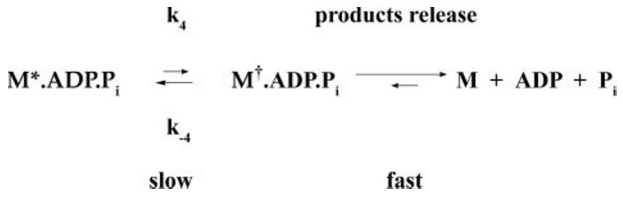

SCHEME 3

following sections we describe step by step how the relevant kinetic parameters were determined.

Separation of the Lever Arm Motion from the Ligand Binding/Release Processes—Previous studies have verified that the measured rate constants of W129+, W501+, and the wild-type motor domain are similar, and thus the introduced mutations do not change the kinetic mechanism significantly (17–19). Because Trp-129 and Trp-501 are located at the nucleotide binding pocket and in the relay helix, respectively, upon ADP and phosphate binding, different local molecular events are detected by following tryptophan fluorescence changes (Fig. 6). To follow ligand binding events, W129+ was mixed with ADP in the presence of 25 mM phosphate, and a large, relatively fast ($k_{ADP,max,app}^{W129+\cdot Pi} = 370\ s^{-1}$) fluorescence decrease was detected. This event is slightly slower than ADP binding in the absence of phosphate. In an earlier study we showed that Trp-129 senses only ligand binding events, and it is insensitive to the conformational changes that occur in the switch 2 and the relay/converter regions. Under the same conditions, when W501+·P_i was mixed with ADP a much slower fluorescence increase ($k_{ADP,max,app}^{W501+\cdot Pi} = 0.20\ s^{-1}$) was detected than in the case of W129+·P_i (Fig. 6). The Trp-501 fluorescence change responds to the large isomerization coupled to the lever arm swing (18). Because the fluorescence change of Trp-129, located at the binding pocket, is much faster than that of Trp-501, located in the relay region, it indicates that ADP and phosphate binding events occur separately from the lever arm swing. Consequently, in the basal ATPase cycle, the rate-limiting step is the slow lever arm swing (M*·ADP·P_i ↔ M†·ADP·P_i) and not the phosphate release step. Thus the supposition in the original Bagshaw-Trentham scheme has been validated (3, 4). In Scheme 3 below, k_{-4} is the rate of the recovery step with bound ADP·P_i (it is important to note that this is different from the k_{+3a} of the recovery step with bound ATP). k_4 is the rate of the reverse recovery step with bound ADP·P_i.

If the slow fluorescence increase of W501+ ($k_{ADP,max,app}^{W501+\cdot Pi}$) is assigned to the lever arm swing, the relaxation of this equilibrium is $k_{ADP,max,app}^{W501+\cdot Pi} = k_4 + k_{-4}$. In the absence of phosphate, the basal ATPase rate constant ($k_{basal} = 0.05\ s^{-1}$) is determined by k_4, therefore $k_{-4} = k_{ADP,max,app}^{W501+\cdot Pi} - k_4 = 0.15\ s^{-1}$, and the equilibrium constant is $K_4 = k_4/k_{-4} = 0.33$. The mechanism is confirmed by the fact that a small, fast fluorescence quench was detected in the reaction when W501+·P_i was mixed with ADP (Figs. 4 and 6). The quench represents the initial M†·ADP·P_i state, which goes through the slow isomerization reaction resulting M*·ADP·P_i state. The rate constant of the fast quench is as fast as the rate constants of ADP binding of W129+·P_i, which also indicates that binding events are being monitored in both cases.

This two-step mechanism is also confirmed by the result of the experiment when dmADP was chased by ATP in the presence of saturating concentration of phosphate (Fig. 7). The observed two phases correspond to the two populations of the M·dmADP·P_i complex. The fast phase is the release of the ligands from M†, and the slow phase represents the reverse recovery step, because shifting this pre-equilibrium (which is established in the preincubation of myosin with ADP and phosphate) becomes the rate-limiting step of the ligand release after the quick release of ADP and phosphate from M†. The ratio of the amplitudes of the two phases ($A_{fast}/A_{slow} = 0.50$) gives the equilibrium constant of the reverse recovery step. Taking the values calculated for the reverse recovery step ($K_4 = 0.33$) and for phosphate affinity for M·ADP complex (K_d,DP = 42 mM), the expected ratio of the amplitudes of the two phases should be $A_{fast}/A_{slow} = 0.78$. The difference from the expectation could be the effect of the mant group of dmADP, which has been demonstrated to affect the affinity of ADP (33–35), and probably influences the binding properties of phosphate as well. If we suppose that the equilibrium between the M*·ADP·P_i and M†·ADP·P_i is not affected by the mant group, then a 2.7-fold stronger binding of phosphate to M·ADP (K_d,DP = 9.6 mM instead of 42 mM) is indicated. On the other hand, if phosphate affinity was unaltered, the equilibrium of the reverse recovery step would change a little: $K_4 = 0.12$ for dmADP instead of 0.33 for ADP.

How Does Actin Activation Occur?—As we showed above, the rate-limiting step of the basal ATPase activity is the reverse recovery step, whereas dissociation of ADP and phosphate is comparatively fast. Previous studies showed that actin causes relatively small changes (2–5 times) in the rate constants of ligand binding/dissociation and of the recovery step (38). Because actin activation causes a 76 times overall increase of the ATPase ($V_{max} = 3.8\ s^{-1}$ from $0.05\ s^{-1}$), the largest effect of actin must be on the rate-limiting step of basal ATPase. Thus, the approximate rate of the actin-induced power stroke is then $k_4' = 76 * k_4 = 3.8\ s^{-1}$ for the A·M*·ADP·P_i → A·M†·ADP·P_i reaction. Note that this reaction starts from the weak actin binding conformation of myosin, in which switch 2 is still closed, however actin binding might induce the opening of the switch 1 loop. Very recently this state was kinetically characterized by Jahn (39) with an ATP analogue (γ-amido-ATP), which favors the closed switch 2 state. He observed actin binding of myosin II with closed switch 2 pre-power stroke conformation. However, k_{-4}' still remains unresolved by a direct experimental measurement, but our simulation results support the assumption that it is very similar to $k_4 = 0.15\ s^{-1}$. Otherwise the flux through the actin-detached M†·ADP·P_i state (see Scheme 4) would dominate the flux via the actin-attached A·M†·ADP·P_i state and lead to wasteful ATP hydrolysis. If we assume that the rate constant of the reverse step of the power stroke (k_{-4}') is approximately the same as that of the reverse step of the reverse recovery step (k_{-4}), *i.e.* $k_{-4}' = k_{-4} = 0.15\ s^{-1}$, then the equilibrium constant for the lever arm movement increases from $K_4 = 0.33$ in the absence of actin to $K_4' = 25$ upon actin-activation. This equilibrium constant represents a $\Delta\Delta G_0 = 10$ kJ/mol difference in free energy change. In other words, actin pushes the equilibrium toward the lever arm-down, post-power

stroke state. This energy change accompanying the swing of the lever arm ($M^* \rightarrow M^\dagger$) is paid for the improved binding to actin, as the K_d goes from 57 μM for A·M*·ADP·P_i to 0.7 μM for A·M†·ADP·P_i, *i.e.* changing by the factor of 81. The strength of actin binding further increases in the following steps of product release: the whole sequence of actin dissociation constants between the pre-power stroke and rigor states decreases as follows: K_d,A·M*·ADP·Pi = 57 μM, K_d,A·M†·ADP·Pi = 0.7 μM, K_d,A·M†·ADP = 0.12 μM, and K_d,A·M = 0.03 μM (40). This stronger actin binding is the driving force that pulls the reaction through the weakly bound A·M*·ADP·P_i state (see Scheme 4). As a consequence, despite the fact that M*·ADP·P_i binds actin very weakly (K_d = 57 μM), the main flux of the reaction occurs via the actin bound form, even if the actin concentration is low (Fig. 8*a*). Our kinetic models show that at 0.5 μM actin concentration, the flux of the actin-bound and -unbound pathways are equal. By increasing actin concentration the ratio of the fluxes dramatically increases: *e.g.* at 5 μM actomyosin concentration the ratio is $Flux_{actin\text{-}bound}/Flux_{actin\text{-}unbound}$ = 14 (Fig. 8*b*).

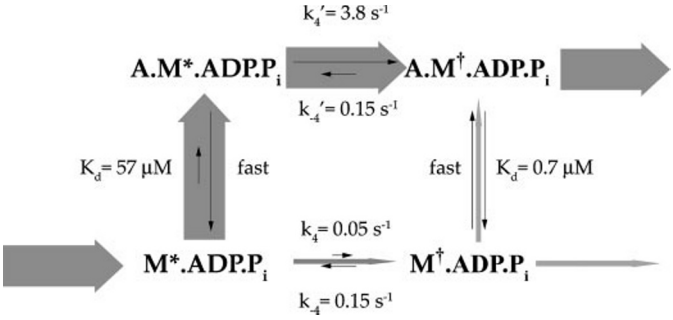

SCHEME 4

In earlier studies, phosphate release was proposed to precede the working-stroke step in the actin-attached states (21, 38, 41) based on the assumption that the A·M*·ADP·$P_i \rightarrow$ A·M†·ADP·P_i transition is not poised strongly to the right, *i.e.* $k_{-4}' \gg k_{-4} = 0.15\ s^{-1}$. If this assumption was valid, this would imply that phosphate release provides the required free energy change for the working stroke, which therefore should precede the lever arm swing avoiding significant futile cycle. This is inconsistent with physiological studies, which have demonstrated significant tension generation before phosphate release, thus demanding significant free energy change from the AM*ADP·P_i to AM†·ADP·P_i transition itself (2, 11–14, 42, 43). Takagi *et al.* (14) also demonstrated in single fiber experiments that the binding of the M·ADP·P_i complex to actin is a fast and weak binding process. They proposed a scheme, which was supported by other studies (11–13) in which the weak actin binding A·M·ADP·P_i state undergoes an isomerization to a strongly bound tension generating state. This is then followed by phosphate release, which might strengthen further the actin-myosin interaction. The model based on solution kinetic measurements presented here is consistent with this mechanism, because they show that the order of events is: weak actin binding occurs first, then the actin activated initiation of the power stroke, and finally the product release steps. However, in contrast to previous studies (14, 44–46), which suggested that the weak-to-strong transition of actin binding should precede the power stroke, our results suggest that the weak-to-strong transition does not necessarily precede the lever arm swing of the power stroke and they might be concurrent processes.

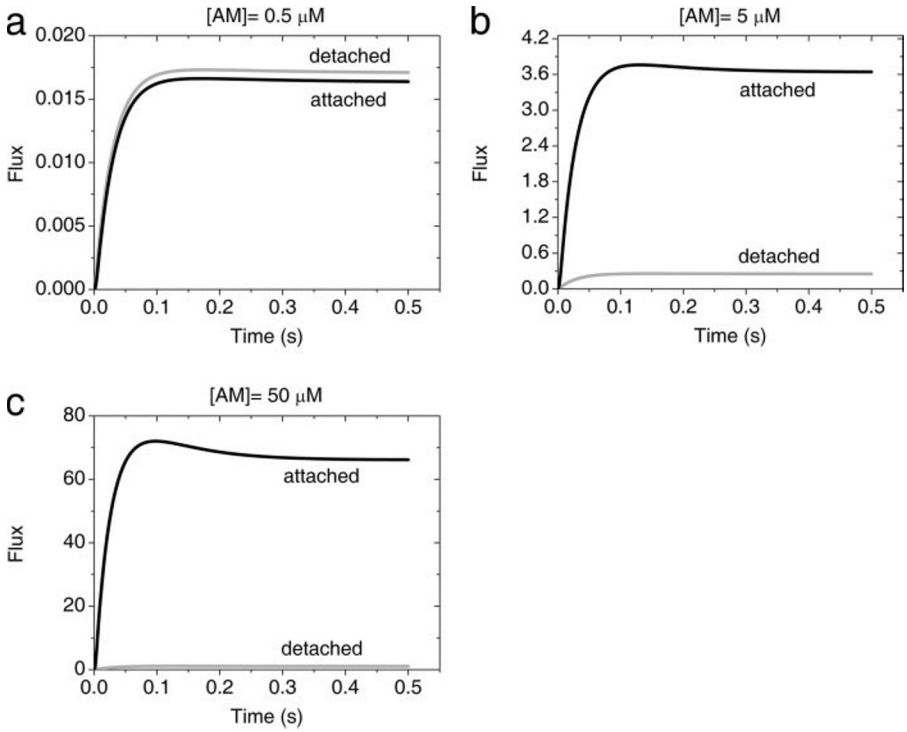

FIGURE 8. **Simulation of the power stroke step at different actin concentrations.** *a*, at low actin concentrations (0.5 μM) the isomerization reaction in the actin attached (*black*) and detached (*gray*) forms are practically equal. *b*, at moderately increased (5 μM) actin concentration >90% of the reaction flux occurs in the actin-bound state; this distribution is further pushed toward the actin attached form at higher (50 μM) actin concentration (*c*). Note the different scaling of the flux on the different panels.

This mechanism also answers another interesting question: if the recovery step that occurs in the M·ATP form is a simple reversal of the power stroke that occurs in M·ADP·P_i, and both nucleotide states have weak actin affinities, why does the first occur in actin detached form, while the latter reaction must happen predominantly in actin-bound form (otherwise a futile cycle would occur)? The answer is that the recovery step is rapid in the absence of actin and is not activated by actin (38), whereas the power stroke step (and not phosphate release) is accelerated by actin, which pulls the reaction flux toward the actin-bound reaction pathway (Scheme 4). In other words, actin activation diverts the reaction flow to the actin-bound pathway inducing the actin-bound power stroke (Fig. 8). Consequently, there is a kinetic reason why the

TABLE 3
Kinetic parameters of the reaction sub-steps measured in this study

	Rate constants	Equilibrium/dissociation constants
$K_{\text{ATP-binding}}$ (55)		120 μM^{-1} (8 nM)
k_{3a} (19)	350 s^{-1}	
k_{-3a} (19)	870 s^{-1}	
K_{3a} (19)		0.40 (2.5)
$K_{\text{hydrolysis}}$ (19)		82 (0.012)
K_{DP} (K_d,DP)		0.024 mM^{-1} (42 mM)
$k_{PD,on}$	1.6 $\mu M^{-1}s^{-1}$	
$k_{PD,off}$	19 s^{-1}	
K_{PD} (K_d,PD)		0.084 μM^{-1} (12 μM)
$k_{P,off}$	260 s^{-1}	
$k_{D,on}$ (17)	1.2 $\mu M^{-1}s^{-1}$	
$k_{D,off}$ (17)	7 s^{-1}	
K_D (K_d,D) (17)		0.17 μM^{-1} (5.8 μM)
k_4	0.05 s^{-1}	
k_{-4}	0.15 s^{-1}	
K_4		0.33
K_d, A·M*·ADP·P_i [a]		57
K_d, A·M†·ADP·P_i [b]		0.7
K_d, A·M†·ADP (40)		0.12
K_d, A·M (40)		0.03

[a] Based on W501+·ADP·AlF_4 pyrene-labeled actin binding experiments.
[b] Calculated value from the thermodynamic box of Scheme 4.

reaction path is diverted to the actin-detached states during the recovery step, while the main flux flows through the actin-bound states in the case of the power stroke. Moreover, the weakly actin-bound A·M*·ADP·P_i and A·$M^{\dagger}$·ADP·P_i states represent higher free energy states compared with those in the detached states (M*·ADP·P_i and $M^{\dagger}$·ADP·P_i, respectively), whose energy can also be utilized upon the power stroke of myosin.

Structural Aspects and Questions—Several questions arise from the present findings. First, is the myosin structure in the M*·ADP·P_i state the same as in the M*·ATP state? Some structural change must account for the fact that the up-down motion of the lever arm is four orders of magnitude slower for M*·ADP·P_i (0.05 s^{-1}) than for M*·ATP (~1000 s^{-1}) (Table 3). By *in silico* experiments the initial events of that structural change have been described recently. Combined quantum/classical molecular mechanics calculations of the ATP hydrolysis reaction path in myosin have shown that the nucleotide reorganizes first, in particular via a motion of the magnesium, which moves between the β and γ phosphate groups, thereby breaking its interaction with the switch 1 loop. This destabilizes the closed switch 1 conformation and prepares for its subsequent opening upon actin binding (47). Molecular dynamics simulations have shown that this is then followed by changes in the hydrogen bond network between the switch 2 loop, the relay helix, and the wedge loop (His-572 through Ala-574), leading to a locking of the wedge loop in the pre-power stroke configuration (48). Because the wedge loop motion is coupled to the lever arm swing (24), this locking can contribute to the much reduced rate of the reverse recovery step from the M*·ADP·P_i state.

Scheme 2 of the basal ATPase raises an intriguing question: Why is the reverse recovery step (k_4, which is the rate-limiting step of the basal ATPase) needed before the products can be released (K_5, K_6, and K_7)? In other words, because switch 1 opening is likely to be needed to allow product release, why can't switch 1 open in the M*·ADP·P_i state of myosin? The reason is that when switch 1 opens, it is coupled to the closing of the actin-binding cleft between the upper and lower 50-kDa domains (49). Although cleft closing can occur freely when the lever arm is "down" (*i.e.* in the pre-recovery step orientation, $M^{\dagger}$), the same closing is not allowed when the lever arm is "up" in M*. In other words, the actin-binding cleft and the lever arm are coupled (note that it is precisely this coupling that drives the power stroke when the cleft closing is induced by actin binding). In the absence of actin, this coupling prevents the closure of the actin-binding cleft, thus preventing the coupled opening of switch 1. Therefore, the pathway of basal ATPase involves first reversal of the recovery step (M*·ADP·P_i → $M^{\dagger}$·ADP·P_i) to allow the combined switch 1 opening/cleft closing, which in turn allows the subsequent release of the products. In addition to switch 1 opening, the release of the γ-phosphate is likely to require also the opening of the switch 2 loop. Because that loop is strongly correlated to the lever arm orientation, another reason for the need of the reverse recovery step is to open switch 2 and allow γ-phosphate release.

When actin binds to M*·ADP·P_i, actin induces closure of the actin-binding cleft and opening of the switch 1 loop (23, 50–54). Takagi *et al.* (14), suggested that the actin-induced opening of switch 1 weakens the interaction between switch 1 and 2, thus letting switch 2 open. This in turn would weaken the binding of the γ-phosphate and allow its release, leading to the increased ATPase turnover rate. But this explanation assumes that switch 2 can open independently from the motion of the lever arm. This is not likely, because, as long as the lever arm is in the pre-power stroke orientation, the wedge loop blocks the opening of switch 2, and the wedge loop is coupled to the lever arm orientation. Therefore, a more complete explanation for the actin-induced acceleration of the ATPase cycle is that actin binding also accelerates the lever arm reorientation (*i.e.* the power stroke), which in turn is coupled to switch 2 opening, thus facilitating the subsequent release of the products.

REFERENCES

1. Geeves, M. A., and Holmes, K. C. (2005) *Adv. Protein Chem.* **71,** 161–193
2. Karatzaferi, C., Chinn, M. K., and Cooke, R. (2004) *Biophys. J.* **87,** 2532–2544
3. Trentham, D. R., Bardsley, R. G., Eccleston, J. F., and Weeds, A. G. (1972) *Biochem. J.* **126,** 635–644
4. Trentham, D. R., Eccleston, J. F., and Bagshaw, C. R. (1976) *Q. Rev. Biophys.* **9,** 217–281
5. Mannherz, H. G., Schenck, H., and Goody, R. S. (1974) *Eur. J. Biochem.* **48,** 287–295
6. Goody, R. S., Hofmann, W., and Mannherz, G. H. (1977) *Eur. J. Biochem.* **78,** 317–324
7. Dantzig, J. A., and Goldman, Y. E. (1985) *J. Gen. Physiol* **86,** 305–327
8. White, H. D., and Taylor, E. W. (1976) *Biochemistry* **15,** 5818–5826
9. White, H. D., Belknap, B., and Webb, M. R. (1997) *Biochemistry* **36,** 11828–11836
10. Goldman, Y. E., and Brenner, B. (1987) *Annu. Rev. Physiol* **49,** 629–636
11. Dantzig, J. A., Goldman, Y. E., Millar, N. C., Lacktis, J., and Homsher, E. (1992) *J. Physiol* **451,** 247–278
12. Kawai, M., and Halvorson, H. R. (1991) *Biophys. J.* **59,** 329–342
13. Kawai, M., and Zhao, Y. (1993) *Biophys. J.* **65,** 638–651
14. Takagi, Y., Shuman, H., and Goldman, Y. E. (2004) *Philos. Trans. R. Soc. Lond. B. Biol. Sci.* **359,** 1913–1920
15. Werber, M. M., Peyser, Y. M., and Muhlrad, A. (1992) *Biochemistry* **31,** 7190–7197
16. Bagshaw, C. R., and Trentham, D. R. (1974) *Biochem. J.* **141,** 331–349
17. Kovacs, M., Malnasi-Csizmadia, A., Woolley, R. J., and Bagshaw, C. R.

(2002) *J. Biol. Chem.* **277,** 28459–28467
18. Malnasi-Csizmadia, A., Woolley, R. J., and Bagshaw, C. R. (2000) *Biochemistry* **39,** 16135–16146
19. Malnasi-Csizmadia, A., Pearson, D. S., Kovacs, M., Woolley, R. J., Geeves, M. A., and Bagshaw, C. R. (2001) *Biochemistry* **40,** 12727–12737
20. Malnasi-Csizmadia, A., Kovacs, M., Woolley, R. J., Botchway, S. W., and Bagshaw, C. R. (2001) *J. Biol. Chem.* **276,** 19483–19490
21. Zeng, W., Conibear, P. B., Dickens, J. L., Cowie, R. A., Wakelin, S., Malnasi-Csizmadia, A., and Bagshaw, C. R. (2004) *Philos. Trans. R. Soc. Lond. B. Biol. Sci.* **359,** 1843–1855
22. Coureux, P. D., Wells, A. L., Menetrey, J., Yengo, C. M., Morris, C. A., Sweeney, H. L., and Houdusse, A. (2003) *Nature* **425,** 419–423
23. Yang, Y., Gourinath, S., Kovacs, M., Nyitray, L., Reutzel, R., Himmel, D. M., O'Neall-Hennessey, E., Reshetnikova, L., Szent-Gyorgyi, A. G., Brown, J. H., and Cohen, C. (2007) *Structure* **15,** 553–564
24. Koppole, S., Smith, J. C., and Fischer, S. (2007) *Structure* **15,** 825–837
25. Mesentean, S., Koppole, S., Smith, J. C., and Fischer, S. (2007) *J. Mol. Biol.* **367,** 591–602
26. Wakelin, S., Conibear, P. B., Woolley, R. J., Floyd, D. N., Bagshaw, C. R., Kovacs, M., and Malnasi-Csizmadia, A. (2002) *J. Muscle Res. Cell Motil.* **23,** 673–683
27. Beynon, R. J., and Easterby, J. S. (1996) *Buffers for pH Control: The Basics*, Bios Scientific Publishers, Oxford
28. Kurzawa, S. E., Manstein, D. J., and Geeves, M. A. (1997) *Biochemistry* **36,** 317–323
29. Manstein, D. J., Schuster, H. P., Morandini, P., and Hunt, D. M. (1995) *Gene* (*Amst.*) **162,** 129–134
30. Pardee, J. D., and Spudich, J. A. (1982) *Methods Cell Biol.* **24,** 271–289
31. Kintses, B., Simon, Z., Gyimesi, M., Toth, J., Jelinek, B., Niedetzky, C., Kovacs, M., and Malnasi-Csizmadia, A. (2006) *Biophys. J.* **91,** 4605–4610
32. Bauer, C. B., Kuhlman, P. A., Bagshaw, C. R., and Rayment, I. (1997) *J. Mol. Biol.* **274,** 394–407
33. Kuhlman, P. A., and Bagshaw, C. R. (1998) *J. Muscle Res. Cell Motil.* **19,** 491–504
34. Woodward, S. K., Geeves, M. A., and Manstein, D. J. (1995) *Biochemistry* **34,** 16056–16064
35. Ritchie, M. D., Geeves, M. A., Woodward, S. K., and Manstein, D. J. (1993) *Proc. Natl. Acad. Sci. U. S. A.* **90,** 8619–8623
36. Goodno, C. C. (1982) *Methods Enzymol.* **85,** 116–123
37. Wells, C., and Bagshaw, C. R. (1984) *J. Muscle Res. Cell Motil.* **5,** 97–112
38. Conibear, P. B., Malnasi-Csizmadia, A., and Bagshaw, C. R. (2004) *Biochemistry* **43,** 15404–15417
39. Jahn, W. (2007) *Biochemistry* **46,** 9654–9664
40. Gyimesi, M., Tsaturyan, A. K., Kellermayer, M. S., and Malnasi-Csizmadia, A. (2008) *Biochemistry* **47,** 283–291
41. Malnasi-Csizmadia, A., Dickens, J. L., Zeng, W., and Bagshaw, C. R. (2005) *J. Muscle Res. Cell Motil.* **26,** 31–37
42. Siththanandan, V. B., Donnelly, J. L., and Ferenczi, M. A. (2006) *Biophys. J.* **90,** 3653–3665
43. Smith, D. A., and Sleep, J. (2004) *Biophys. J.* **87,** 442–456
44. Lionne, C., Brune, M., Webb, M. R., Travers, F., and Barman, T. (1995) *FEBS Lett.* **364,** 59–62
45. Lionne, C., Iorga, B., Candau, R., Piroddi, N., Webb, M. R., Belus, A., Travers, F., and Barman, T. (2002) *Biochemistry* **41,** 13297–13308
46. Tesi, C., Colomo, F., Piroddi, N., and Poggesi, C. (2002) *J. Physiol.* **541,** 187–199
47. Schwarzl, S. M., Smith, J. C., and Fischer, S. (2006) *Biochemistry* **45,** 5830–5847
48. Koppole, S., Smith, J. C., and Fischer, S. (2006) *J. Mol. Biol.* **361,** 604–616
49. Kintses, B., Gyimesi, M., Pearson, D. S., Geeves, M. A., Zeng, W., Bagshaw, C. R., and Malnasi-Csizmadia, A. (2007) *EMBO J.* **26,** 265–274
50. Conibear, P. B., Bagshaw, C. R., Fajer, P. G., Kovacs, M., and Malnasi-Csizmadia, A. (2003) *Nat. Struct. Biol.* **10,** 831–835
51. Rayment, I., Holden, H. M., Whittaker, M., Yohn, C. B., Lorenz, M., Holmes, K. C., and Milligan, R. A. (1993) *Science* **261,** 58–65
52. Rayment, I., Rypniewski, W. R., Schmidt-Base, K., Smith, R., Tomchick, D. R., Benning, M. M., Winkelmann, D. A., Wesenberg, G., and Holden, H. M. (1993) *Science* **261,** 50–58
53. Reubold, T. F., Eschenburg, S., Becker, A., Kull, F. J., and Manstein, D. J. (2003) *Nat. Struct. Biol.* **10,** 826–830
54. Schroder, R. R., Manstein, D. J., Jahn, W., Holden, H., Rayment, I., Holmes, K. C., and Spudich, J. A. (1993) *Nature* **364,** 171–174